

UGC 1378 – a Milky Way-sized galaxy embedded in a giant low-surface brightness disc

Anna S. Saburova,^{1,2}  Igor V. Chilingarian,^{3,1} Anastasia V. Kasparova,¹ Ivan Yu. Katkov,^{1,4} Daniel G. Fabricant,³ Roman I. Uklein,⁵

¹ Sternberg Astronomical Institute, Moscow M.V. Lomonosov State University, Universitetskij pr., 13, Moscow, 119234, Russia

² Institute of Astronomy, Russian Academy of Sciences, Pyatnitskaya st., 48, 119017 Moscow, Russia

³ Smithsonian Astrophysical Observatory, 60 Garden Street MS09, Cambridge, MA 02138, USA

⁴ New York University Abu Dhabi, Saadiyat Island, PO Box 129188, Abu Dhabi, UAE

⁵ Special Astrophysical Observatory, Russian Academy of Sciences, Nizhniy Arkhyz, Karachai-Cherkessian Republic 357147, Russia

2 September 2019

ABSTRACT

The dominant physical processes responsible for the formation and longevity of giant gaseous and stellar discs in galaxies remain controversial. Although they are rare (less than 10 confirmed as of now), giant low-surface brightness (gLSB) discy galaxies provide interesting insights given their extreme nature. We describe observations of UGC 1378 including deep spectroscopy with the Russian 6m telescope and multi-band imaging with Binospec at the MMT. Galaxy UGC 1378 has both high surface brightness and an extended low surface brightness discs. Our stellar velocity dispersion data for the high-surface brightness, Milky Way-sized, disc appears inconsistent with a recent major merger, a widely discussed formation scenario for the very extended low surface brightness disc. We estimate the star formation rates (SFR) from archival Wide-Field Infrared Survey Explorer data. The SFR surface density in the LSB disc is low relative to its gas density, consistent with recent gas accretion. We argue that the unusually large size of UGC 1378’s disc may be the product of a rich gas reservoir (e.g. a cosmic filament) and an isolated environment that has preserved the giant disc.

Key words: galaxies: kinematics and dynamics, galaxies: evolution

1 INTRODUCTION

We report observations of an unusual massive gas-rich galaxy, UGC 1378, with extended (radii ~ 50 kpc) gaseous and low-surface brightness stellar discs (Mishra et al. 2017). We build upon our previous studies of giant low-surface brightness galaxies (gLSB) in Kasparova et al. (2014) and Saburova et al. (2018). These galaxies deserve special attention because the formation of a $\sim 10^{12} M_{\odot}$ disc galaxy is not easily explained in the hierarchical clustering paradigm. Major merger events are expected to destroy large discs but in simulations the merger trees of $10^{12} M_{\odot}$ haloes almost always include major mergers (Rodríguez-Gomez et al. 2015). We would like to understand how these large discs form, how they managed to survive, and whether there is a continuum of properties between gLSB and HSB galaxies. Studies of gLSB galaxies can also help us to understand the importance of gas accretion and outflows.

UGC 1378 is classified as a type-SBa gLSB system (Schombert 1998) and is especially intriguing because its H I content is higher than expected relative to its stellar mass (according to the relation in Wang et al. 2013). Our deep imaging reveals the complex

structure of UGC 1378, including a high-surface brightness (HSB) bulge and disc, and a gLSB disc. In common with other gLSB-Gs, UGC 1378 has prominent spiral arms (like Malin 1, Malin 2, UGC 1922, UGC 1382, Boissier et al. 2016; Galaz et al. 2015; Hagen et al. 2016; Kasparova et al. 2014; Saburova 2018), resembling the Milky Way immersed in a gLSB disc.

Formation scenarios for gLSBs include: (i) a major merger (Zhu et al. 2018; Saburova et al. 2018) in which an extended disc is formed from an ample supply of gas cooled down at the late stage of a merger; (ii) a gradual build-up of a gLSB disc by minor mergers with gas-rich satellites (Peñarrubia et al. 2006); (iii) a build-up of a gLSB disc by accretion from cosmic filaments (Saburova et al. 2018); (iv) a non-catastrophic scenario in which the peculiar structure of a gLSB is created because of the large radial scale and low central density of a dark halo (Kasparova et al. 2014).

Accretion of intergalactic gas is required to explain star formation rates in disc galaxies (Larson et al. 1980) and also affects the angular momentum of galactic discs (see, e.g. Stewart 2017, and references therein). The kinematics of extended disc-like structures traced by cold gas around galaxies at $z \approx 1$ is consistent with a cold accretion model (Zabl et al. 2019). There is meagre direct observational evidence for accretion in massive galaxies at low redshifts

* E-mail: saburovaann@gmail.com

(see, e.g. Oosterloo et al. 2007; Vollmer et al. 2016; Fraternali et al. 2001, 2002; de Blok et al. 2014) even though in low-mass galaxies it is more commonly observed (see, e.g. Kirby et al. 2016; Schmidt et al. 2014; Józsa 2007). At the same time, the radial distribution of the oxygen effective yield in massive spirals indicates that accretion of metal poor-gas must be higher in larger galaxies (Zasov et al. 2015). Searches for accretion in massive H I excess galaxies may therefore be productive.

H I excess galaxies have been the focus of previous studies. The “Bluedisk” project (Wang et al. 2013) mapped the H I distribution in 23 nearby galaxies with unusually high H I mass fractions, finding an H I excess in the surrounding environment (Wang et al. 2015). Kinematical studies of ‘Bluedisk’ galaxies did not reveal enhanced global asymmetry of the H I-excess galaxies relative to the control sample, a possible indication of accretion (den Heijer et al. 2015). A study of five H I excess galaxies with inefficient star formation and stellar masses $> 10^{10} M_{\odot}$ gas by Geréb et al. (2018) suggested an external gas origin in two cases and an ambiguous gas origin in the other cases. UGC 1378 is more massive than most of the “Bluedisk” galaxies and has a redshift roughly half the “Bluedisk” mean. UGC 1378’s gas-to-stellar mass ratio, its H I disc size and mass are similar to the “Bluedisk” galaxies. UGC 1378’s H I mass fraction is lower than that of the galaxies in the Geréb et al. (2018) and HighMass (Huang et al. 2014) samples. UGC 1378’s properties are summarized in Table 1.

Like most other gLSBs, UGC 1378 is located in a low-density environment (Saburova et al. 2018), therefore the dynamical disturbances from a dense environment are minimized and it is easier to search for cold accretion. The Saulder et al. (2016) group catalogue contains no spectroscopically confirmed companions for UGC 1378 and our deep photometry reveals no satellites with g surface brightness higher than $26 \text{ mag arcsec}^{-2}$ within 80 kpc. The sparse environment may be the key factor to the survival of a large low-surface brightness disc even though it does not necessarily mean that the galaxy grew in isolation throughout the cosmic time. UGC 1378 may have accreted the absent satellites. However, the accretion did not transform UGC 1378 into an early-type galaxy (see, e.g. Deeley et al. 2017) and it remains a discy system. We suggest that UGC 1378 may have formed in two stages. The first stage, in common with MW-type galaxies, may have included several episodes of merging and a second stage, following the accretion of most satellites, quiescently formed gLSB stellar and gaseous discs by accretion of metal-poor gas from a cosmic filament.

This paper is organized as follows: Section 2 describes long-slit spectral and photometric observations and data reduction; the results of the data analysis are given in Section 3; our mass modelling, which estimates the masses of the discs, bulge and dark matter halo is described in Section 3.3; we discuss the results in Section 4; and summarize our findings in Section 5.

2 OBSERVATIONS AND DATA REDUCTION

2.1 Long-slit spectral observations

We observed UGC 1378 with the SCORPIO focal reducer/spectrograph (Afanasiev & Moiseev 2005) at the prime focus of the 6-m Russian telescope on 20 September 2017 using a 6-arcmin long and 1 arcsec wide slit, and the VPH G2300G grism. This setup provides spectral coverage from 4800-5570 Å, dispersion of $0.38 \text{ Å pixel}^{-1}$, with an instrumental FWHM of 2.2 Å . The plate scale along the slit is $0.36 \text{ arcsec pixel}^{-1}$. The total on-source

Table 1. Basic properties of UGC 1378.

References: [1] NED (<http://ned.ipac.caltech.edu>), [2] Mishra et al. (2017).

Names	UGC 1378	ref.
	PGC 007247	
	CGCG326-002	
Equatorial coordinates (J2000.0)	01h56m19.2s +73d16m58s	[1]
Distance	38.8 Mpc	[2]
Morphological type	SBa	[1]
Inclination angle	59°	[2]
Major axis position angle	181°	[2]
H I mass	$1.2 \times 10^{10} M_{\odot}$	[2]
Rotation velocity	282 km s^{-1}	[2]
Scale kpc/arcsec	0.188	

exposure time was 7 hours in 1.4 arcsec seeing. The slit was oriented along the major axis of UGC 1378 at $PA = 181^{\circ}$ (Mishra et al. 2017). We used spectra of on-board arc and flat field lamps for calibration.

We reduced the spectral data using our IDL based pipeline. The data reduction steps include: bias subtraction and overscan clipping, flat-field correction, wavelength calibration¹, cosmic ray removal, linearization, and co-addition of multiple exposures. Night sky subtraction used the algorithm described in Katkov & Chilingarian (2011) and flux calibration used observations of the spectrophotometric standard star *BD 25+4655*.

We measured the instrumental line-spread function of the spectrograph along the slit throughout the observed wavelength range, by fitting a twilight sky spectrum (observed in the same night) to a high-resolution Solar spectrum using PPIXF (Cappellari & Emsellem 2004). We then fitted the reduced spectra of UGC 1378 with intermediate-resolution ($R = 10000$) PEGASE.HR (Le Borgne et al. 2004) simple stellar population models (SSP) for Salpeter IMF (Salpeter 1955) convolved with the instrumental line-spread function using the NBURSTS full spectral fitting technique (Chilingarian et al. 2007a,b). The fitting procedure returns the best-fitting parameters of an SSP model, that is age T (Gyr) and metallicity $[\text{Fe}/\text{H}]$ (dex) of stellar population. We parametrized the line-of-sight velocity distribution (LOSVD) of stars by Gauss-Hermite series (see van der Marel & Franx 1993). We obtained a luminosity-weighted stellar age and metallicity, line-of-sight velocity, velocity dispersion and Gauss-Hermite moments h_3 and h_4 which characterize the deviation of LOSVD from the Gaussian profile. We set h_3 and h_4 as zero starting from $\pm 15 \text{ arcsec}$, since we were not able to define reliably these parameters at large galactocentric distances. We defined spatial bins along the slit for the fitting manually by first running an automatic 1D adaptive binning procedure and then adjusting the bin sizes to handle the sharp change in the surface brightness along the slit. We separately analyzed the emission spectrum obtained by subtracting the best-fit stellar populations from the observed spectra. We fitted emission lines to a single Gaussian profile and derived the velocity and velocity dispersion of the ionised gas.²

¹ To improve the wavelength solution accuracy we took arc spectra every 2 h and used them to reduce the corresponding science frames.

² The results of the spectral data analysis in txt-format are available via <https://doi.org/10.5281/zenodo.3352306>



Figure 1. Composite r , g , z -band image of UGC 1378. North is up, east is left, the image size is 7.2×10.1 arcmin.

2.2 Photometric observations

We observed UGC 1378 in the g, r, z bands with the Binospec spectrograph/imager (Fabricant et al. 2019) mounted at the 6.5-meter converted MMT at Mt. Hopkins, Arizona during the Binospec commissioning run on 15 November 2017. The images were reduced using the Binospec pipeline (Kansky et al. 2019). The reduction included cosmic ray cleaning, flat-fielding, alignment of images, illumination correction, co-adding of image stacks, astrometric calibration using SCAMP and re-mapping to the tangential projection using SWARP (Bertin et al. 2002). After that we subtracted the sky with an IDL code. We performed the aperture photometry of stars visible in the images and matched them against the sources in the Data Release 1 of the Pan-STARRS1 Survey (PS1, Chambers et al. 2016). Fig. 1 is our composite g, r, z image of UGC 1378.

3 DATA ANALYSIS RESULTS

3.1 Radial profiles of kinematics and stellar populations

Fig. 2 summarizes our spatially resolved spectral results. The top panel displays the orientation of the long slit along UGC 1378’s major axis. The second panel from the top displays the line-of-sight gas and stellar velocities along the slit, while the third panel plots the gas and stellar velocity dispersions. The strong velocity gradient in the stellar velocity profile indicates a strong bar (see, e.g. Saburova et al. 2017) that is also apparent in the image. The presence of

the bar is also evident in the fourth panel in the radial profiles of stellar Gauss-Hermite moments h_3 and h_4 that characterize the LOSVD deviation from Gaussian. The h_3 profile anticorrelates with radial velocity in the inner region, typical of galaxies with boxy or peanut-shaped bulges (Chung & Bureau 2004). This behaviour of h_3 is also found in galaxies with an inner disc or a ring (see, e.g. Seidel et al. 2015). The central high velocity dispersion and old metal-rich stellar population (see, Fig. 2, two bottom panels) are, however, inconsistent with a kinematically cold young stellar component in the inner part expected with a star-forming ring. The central minimum of the h_4 profile is also reproduced in numerical simulations of a barred galaxy (Saburova et al. 2017). In the centre of UGC 1378 we see a (pseudo-)bulge (see below) dominated by old, metal-rich stars, formed due to the presence of the bar (Kormendy & Kennicutt 2004).

3.2 Light profile decomposition

We fitted two dimensional models to the deep g, r, z -band images. UGC 1378 is located at 11° galactic latitude so that variable Galactic extinction could introduce systematic errors if we attempt one dimensional fits to the radial profile. We use GALFIT (Peng et al. 2002) to fit three structural components, (i) a Sersic bulge (Sersic 1968), parametrized by the central surface brightness $(I_0)_b$, the effective (half-light) radius R_e , and the Sersic index n ; (ii) two exponential discs defined by the central surface brightness $(I_d)_0$ and the exponential scale length R_d . The observed profile is poorly described by a model with a single disc and Sersic bulge, which is evident from Fig. 3 where we show the g -band azimuthally averaged profile of surface brightness³ which is in a good agreement with the results of 2D fitting with two discs. Thus we include a second disc. We masked foreground stars and the outer ring of the bar with $r = 2$ kpc. The derived parameters from the 2D decomposition are listed in Table 2⁴. The magnitudes in Table 2 are corrected for Galactic extinction but not for inclination. The error-bars obtained using GALFIT should be treated with caution since they could be significantly underestimated (see, e.g. Zhao et al. 2015), in our 1D fit we obtained the error of 3-6 percent for the radial scales of HSB disc and bulge, 1 percent error for Sersic index, about 20 percent for the scale of LSB disc and up to 0.1 mag arcsec⁻² for the surface brightnesses which is more reasonable. We note that the central surface brightness of the second disc appears to be higher than the usually adopted B-band LSB limit of >22 mag arcsec⁻² (cf. the 21.65 ± 0.3 range found by Freeman (1970) in HSB galaxies; O’Neil et al. (1997)). However our direct g -band estimate is affected by Galactic cirrus. The r -band measurement is more reliable, 21.54 mag arcsec⁻², corresponding to 21.84 in the g -band using a $(g - r)$ colour of 0.3 mag for the LSB-disc (see the colour map below). We obtain a B-band central surface brightness $\mu_{0,B} = 22.14$ mag arcsec⁻² using transformations from Jester et al. (2005). Hence, the second disc of UGC 1378 satisfies the LSB

³ We calculated a surface brightness profile from the g -band image using the ELLIPSE routine (Jedrzejewski 1987) in the IRAF software environment (Tody 1986).

⁴ We compared the results of 2D fitting with that following from the decomposition of the surface brightness profiles using Levenberg-Marquardt non-linear least-squares IDL routine (Chilingarian et al. 2009) and found a good agreement which could evidence in favour of the reliability of our 2D modelling. The good agreement between 1D and 2D fittings is also evident from Fig. 3 where the 2D model does not deviate from the 1D profile except for the outer region which is effected by the Galactic cirrus.

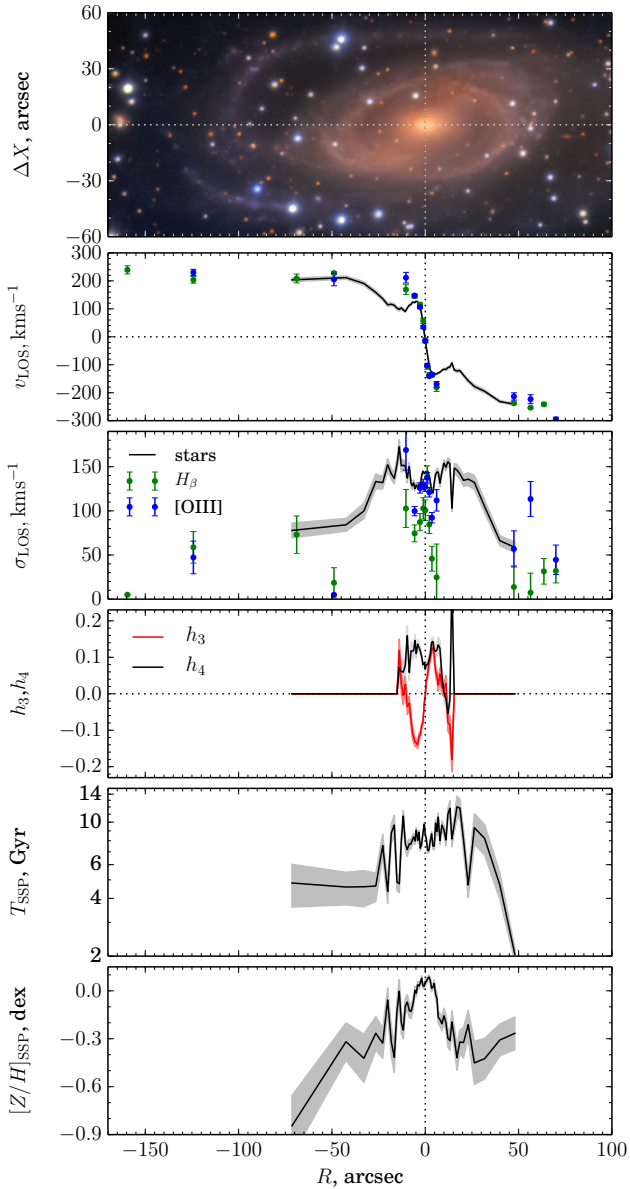


Figure 2. The radial profiles of kinematics and stellar populations of UGC 1378 ($PA = 181^\circ$). From top to bottom: the slit position overlaid on a composite grz -image; LOS velocity of ionized gas measured in $H\beta$ and $[OIII]$ lines (circles) and stars (solid line and shaded areas are for values and their uncertainties), the adopted systemic velocity is 2930 km s^{-1} ; LOS velocity dispersion of gas (circles) and stars (line); h_3 and h_4 Gauss-Hermite coefficients; SSP-equivalent age of stellar population; SSP-equivalent metallicity of stellar population.

central surface brightness criterion despite being brighter than e.g. Malin 1’s disc (Boissier et al. 2016). In the r band, the radius of the LSB disc (4 disc radial scale lengths, Kregel & van der Kruit 2004) is 268 arcsec or 50 kpc, which is similar to that of the $H\text{I}$ disc (45 kpc). The radius of the HSB disc $4(R_d)_r \approx 18$ kpc, which is roughly half of the $H\text{I}$ disc radius. The bulge Sersic index is ~ 1 indicating that UGC 1378 possesses a pseudo-bulge.

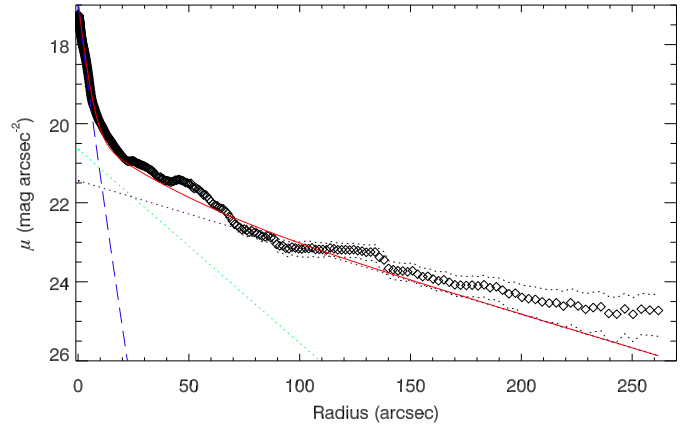


Figure 3. The g -band surface brightness profile of UGC 1378 with an overplotted best-fitting GALFIT model. HSB and LSB discs are shown as green and brown lines, bulge as a blue line. The profiles are corrected for Galactic extinction and are not corrected for inclination.

3.3 Mass-modelling of the rotation curve

We built UGC 1378’s composite rotation curve using $H\text{I}$ (Mishra et al. 2017) and ionized gas (this work) to measure the dynamical masses and sizes of its structural components. For the optical data analysis we use the inclination value adopted by Mishra et al. (2017) for their $H\text{I}$ data. Our rotation curve, derived from emission lines of ionized gas, is in good agreement with the $H\text{I}$ data in the region where the two datasets overlap (see Fig. 3.3, bottom panel, where we show $H\text{I}$ data and ionized gas with crosses and dots, respectively). We decomposed the composite rotation curve into two stellar exponential discs (HSB and LSB), a Sersic bulge, a dark matter halo, and a gas disc⁵. The weights of $H\text{I}$ and optical data points for the fitting procedure were taken from the error-bars shown in the bottom panel of Fig. 3.3. The low S/N optical rotation curve data at $r > 100$ arcsec were not used for mass modelling.

The rotation curves of the components were constructed as in Saburova et al. (2016). We used the following dark halo density profiles:

(i) a Burkert density profile Burkert (1995):

$$\rho_{\text{burk}}(r) = \frac{\rho_0 R_s^3}{(r + R_s)(r^2 + R_s^2)}. \quad (1)$$

Here ρ_0 and R_s are the central density and the radial scale of the halo⁶.

(ii) a pseudo-isothermal profile (hereafter, piso):

$$\rho_{\text{piso}}(r) = \frac{\rho_0}{(1 + (r/R_s)^2)}. \quad (2)$$

(iii) a Navarro-Frenk-White profile Navarro et al. (1996) (hereafter, NFW):

$$\rho_{\text{nfw}}(r) = \frac{\rho_0}{(r/R_s)(1 + (r/R_s)^2)^2}. \quad (3)$$

It is important to constrain the contributions of the stellar disc

⁵ We calculated the $H\text{I}$ surface density from the 0th moment maps from Mishra et al. (2017) using ELLIPSE routine and took into account the expected contribution of helium (multiplied the $H\text{I}$ surface density by 1.3).

⁶ Below R_s and ρ_0 are different for the various DM density profiles.

Table 2. The photometric parameters of the two discs and the bulge of UGC 1378 estimated from a two-dimensional GALFIT decomposition, brightnesses are corrected for extinction following (Schlafly & Finkbeiner 2011) but not corrected for the inclination: central bulge surface brightness $(\mu_0)_b$; bulge effective radius R_e ; bulge Sersic index n ; HSB exponential disc central surface brightness $(\mu_0)_d$; HSB disc radial scale length R_d ; LSB exponential disc central surface brightness $(\mu_0)_{d2}$; LSB disc radial scale length R_{d2} . The scale is $0.188 \text{ kpc arcsec}^{-1}$.

Band	$(\mu_0)_b$ (mag arcsec $^{-2}$)	R_e (arcsec)	n	$(\mu_0)_d$ (mag arcsec $^{-2}$)	R_d (arcsec)	$(\mu_0)_{d2}$ (mag arcsec $^{-2}$)	R_{d2} (arcsec)
<i>g</i>	16.90 ± 0.00	4.30 ± 0.01	1.10 ± 0.01	20.64 ± 0.00	22.13 ± 0.05	21.44 ± 0.00	64.16 ± 0.09
<i>r</i>	16.06 ± 0.00	4.24 ± 0.01	1.05 ± 0.00	19.88 ± 0.00	24.00 ± 0.03	21.54 ± 0.00	66.97 ± 0.15
<i>z</i>	15.72 ± 0.00	4.48 ± 0.01	1.00 ± 0.00	19.13 ± 0.00	22.34 ± 0.03	21.04 ± 0.01	63.92 ± 0.18

and bulge to the total mass because the rotation curve decomposition is ambiguous (see, e.g. Saburova et al. 2016). We are able to limit the disc mass using the marginal gravitational stability criterion from stellar velocity dispersion measurements beyond two disc radial scale lengths from the centre (see, e.g. Zasov et al. 2004; Saburova 2011; Saburova & Zasov 2013). The majority of late-type disc galaxies and some S0 galaxies have discs that are marginally gravitationally stable at two disc radial scale lengths (Zasov et al. 2011).

We formulate the stability criterion as follows. A single component isothermal disc is locally marginally stable when the radial stellar velocity dispersion σ_r at the distance from the centre R is equal to the critical value:

$$(\sigma_r)_{\text{crit}} = Q_T \cdot 3.36G\Sigma_d/\kappa, \quad (4)$$

where κ is the epicyclic frequency, Σ_d is the disc surface density and Q_T is Toomre’s stability parameter (equal to unity for pure radial perturbations of a thin disc). Numerical simulations of the marginal stability of finite thickness exponential discs show that the parameter $Q_T \approx 1.2-3$ slowly increases with radius (see e.g. Khoperskov et al. 2003). The presence of a cold gaseous component can make a disc less stable (see, e.g. Romeo & Wiegert 2011), but the gas surface density in UGC 1378 at two HSB disc radial scalelengths is roughly 20 times lower than that of the stars, so this effect is negligible. The situation is complicated by the presence of the stellar LSB disc. According to the mass-modelling of the rotation curve (see below), its density may be only 2 – 3 times lower than the HSB disc at this radius, so the LSB disc can influence the stability if its velocity dispersion differs significantly from that of HSB disc. Unfortunately, our data are not deep enough to trace the stellar velocity dispersion at the radii where the LSB disc dominates the surface brightness to evaluate its effect on the stability.

We estimate the radial velocity dispersion from the observed line-of-sight stellar velocity dispersion σ_{obs} taking into account the expected links between the dispersion along the radial, azimuthal and vertical directions:

$$\sigma_{\text{obs}}^2(r) = \sigma_z^2 \cdot \cos^2(i) + \sigma_\phi^2 \cdot \sin^2(i) \cdot \cos^2(\alpha) + \sigma_r \sin^2(i) \cdot \sin^2(\alpha), \quad (5)$$

where α is the angle between the direction of the slit and the major axis.

To solve the equation we used two additional conditions: $\sigma_r = 2\Omega \cdot \sigma_\phi/\kappa$ (Lindblad formula for the epicyclic approximation) and $\sigma_z = k \cdot \sigma_r$. The coefficient k was taken to be 0.6 based on direct measurements that give an expected range 0.5–0.8 (see e.g. Shapiro et al. 2003). We estimated the epicyclic frequency from the combined optical and H I rotation curve (Mishra et al. 2017) using

the equation: $\kappa(r) = 2v(r)/r \sqrt{0.5 + r/2v(r)(\frac{\partial v(r)}{\partial r})}$. We used the radial variation of the parameter Q_T resulting from the numerical simulations by Khoperskov et al. (2003).

The central surface density of the HSB disc, extrapolated from an exponential model with the photometric scale length, and using the marginal gravitational stability criterion at two radial scale lengths is roughly $1000 M_\odot \text{ pc}^{-2}$. This surface density corresponds to a disc *r*-band mass-to-light ratio $(M/L_d)_r = 2.88(M/L)_\odot$. This mass-to-light ratio is higher than the ratio obtained from the colour index of the disc and the model relations from Roediger & Courteau (2015): $(M/L_d)_r = 1.02$ and from Bell et al. (2003): $(M/L_d)_r = 1.7$. However, a $(M/L_d)_r = 2.88$ is lower than an estimate of $(M/L_d)_r = 3.3$ based on a Salpeter stellar initial mass function, a stellar population age of 5 Gyr, a metallicity of $[\text{Fe}/\text{H}] = -0.3$ dex (see Fig. 2) and allowing for a gas contribution. Thus, we conclude that the disc of UGC 1378 is close to marginal gravitational stability, suggesting that merger-induced strong gravitational perturbations did not occur after the formation of the HSB disc.

During the modelling of the rotation curve, we fix the radial scales of the discs and the bulge from the *r*-band photometric parameters and the mass-to-light ratio of the HSB disc to 1.4, which follows from the colour index using the relations of Roediger & Courteau (2015), Bell et al. (2003). We allow the mass-to-light ratios of bulge and LSB disc to be free parameters. We summarize the results of the rotation curve mass-modelling in Fig. 4. Following Saburova et al. (2016) we calculate χ^2 maps for the dark halo parameters, also presented in Fig. 4. We give our fits to the structural components of UGC 1378 in Table 3. The combined mass of the two discs is 2.9 – 3.8 times less than the mass of the dark halo inside the LSB and H I discs, higher than for normal HSB galaxies. However, inside the HSB disc, the ratio of dark to luminous matter is close to two as expected for normal galaxies (Zasov et al. 2011). The NFW halo scale radius is large ($>10 \text{ kpc}$), but consistent with the large disc radius (see, e.g. Saburova 2018).

4 DISCUSSION

UGC 1378 has a complex structure as evident in Fig. 1 and from our photometric analysis, with a HSB inner disc and a LSB outer disc with prominent spiral arms. Fig. 5, where we demonstrate the WISE band 3 and *r*-band images of UGC 1378 with overlaid contours of H I density map taken from Mishra et al. (2017), shows that the HSB disc has roughly half the extent of the H I disc, while the LSB disc extends to the edge of the H I disc. The H I contours trace the spiral arms visible in the *r*-band. The inner HSB region of UGC 1378 contains a large-scale bar with an embedded nuclear star-forming ring revealed by a circular red dust lane with a radius of

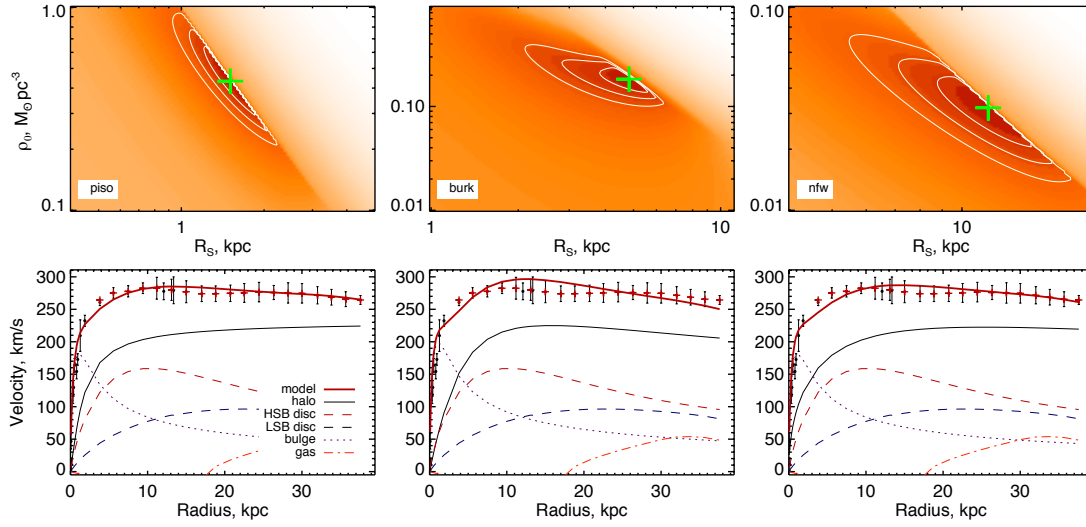


Figure 4. Top panels: χ^2 map for the parameters of dark halo, the darker the colour, the lower the χ^2 and the better the fitting quality is. The contours refer to 1σ , 2σ and 3σ confidence limits. The parameters corresponding to the χ^2 minimum are shown by a cross in each map. Left column — for the piso profile of the DM halo, centre — to the Burkert profile, right — for the NFW profile. Bottom panels: the best-fitting models of the combined H I (red crosses) + optical (black dots) rotation curve.

Table 3. The derived parameters of the main galaxy components with 1σ confidence limit errors. The columns contain the following data: (1) – dark halo profile; (2) and (3) – radial scale and central density of the DM halo; (3) – mass of DM halo inside of radius 47 kpc; (4) – disc r mass-to-light ratio; (5) – central surface density of bulge (6) – LSB and HSB discs mass;

dark halo	R_s kpc	ρ_0 $10^{-3} M_\odot/\text{pc}^3$	M_{halo} $10^{10} M_\odot$	M/L M_\odot/L_\odot	$(I_0)_b$ $10^3 M_\odot/\text{pc}^2$	M_{discs} $10^{10} M_\odot$
Burkert	4.83 +0.36 -0.45	183.38 +46.79 -43.77	41.28 +4.27 -14.85	1.08 +1.89 -0.00	21.77 +0.00 -0.00	14.4
NFW	11.51 +2.94 -2.04	31.99 +13.36 -11.43	50.38 +5.34 -16.14	1.08 +1.78 -0.00	18.13 +0.00 -0.00	14.4
piso	1.51 +0.34 -0.28	432.88 +209.93 -134.51	55.18 +2.70 -7.65	1.08 +0.82 -0.00	18.13 +0.0 -0.00	14.4

10 arcsec (2 kpc). The dust lane is visible in Fig. 6 where we show the $g-r$ colour map of UGC 1378 obtained using adaptive binning to reach signal-to-noise level of 6 and corrected for Galactic extinction (assumed to be constant with radius). This ring is also visible in the stellar velocity dispersion profile (see Fig. 2) with two symmetric peaks that coincide with the edge of the ring. This structure is typical for barred galaxies and occurs in 20% of disc galaxies. The ring may result from a recent gas inflow to the centre of the galaxy (Comerón et al. 2010) but the ring is larger than in most cases described by Comerón et al. (2010). The bar is surrounded by red spiral arms that form a ring-like structure. Our spectral analysis shows that the stellar population in the outer HSB region is metal-poor and is significantly younger than the bar and pseudo-bulge population.

4.1 On the star formation rate of UGC 1378

The low surface brightness outer spiral arms have bluer $g-r$ colour (see Fig. 6) which may indicate a young stellar population. Both the HSB disc and outer spirals are clearly visible in WISE (Wright et al. 2010) band 3 ($\lambda = 12\mu\text{m}$), see Fig. 5. This image supports

the presence of current star formation in the outer gLSB disc of UGC 1378.

We derive the star formation rate (SFR) for UGC 1378 by applying the relations from Jarrett et al. (2013) to the integrated UGC 1378 luminosity at 12 and $22\mu\text{m}$. The global SFR is estimated at between 1.2 and $2.3 M_\odot \text{yr}^{-1}$. This SFR is comparable or higher than the SFR in well-studied nearby galaxies (see, e.g. Jarrett et al. 2013) and is close to the Milky Way SFR (see, f.e., Licquia & Newman 2015; Chomiuk & Povich 2011). However, accounting for the high H I mass (Mishra et al. 2017), this SFR value is in good agreement with the H I mass vs. SFR relation found by Boissier et al. (2008) for other LSB galaxies. They find LSB galaxies have a lower SFR at a given gas mass than HSB galaxies. The SFR in UGC 1378 is also lower than expected from the SFR vs H I mass relation for Local Volume galaxies (Karachentsev & Kaisin 2010). However, the Local Volume galaxies do have much lower gas masses than UGC 1378.

The mean SFR density is $(2 \pm 0.1) \times 10^{-3} M_\odot \text{yr}^{-1} \text{kpc}^{-2}$ which is higher than that observed in LSB galaxies (see, e.g. Wyder et al. 2009). As expected, the LSB spiral arms in UGC 1378 have

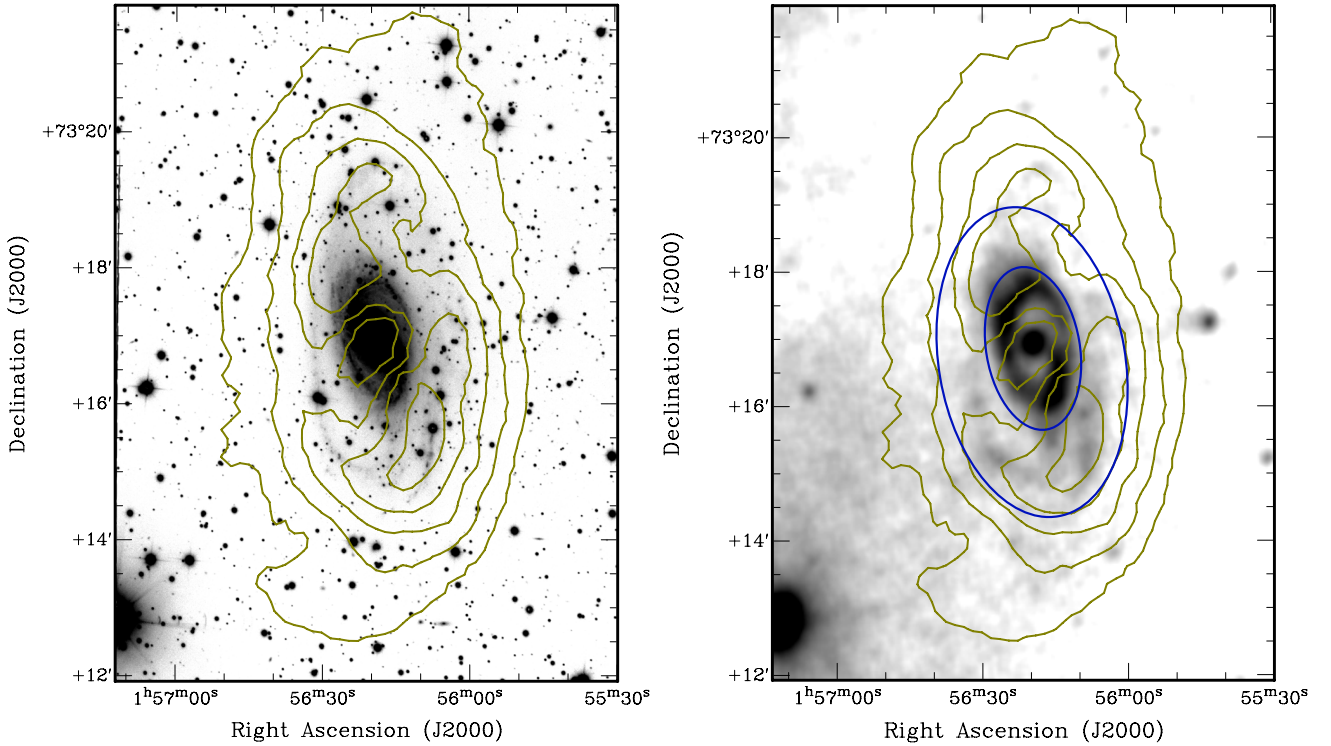


Figure 5. The r -band (left-hand column) and WISE band 3 (right-hand column) images of UGC 1378 with overlaid contours of H I density map taken from Mishra et al. (2017) and areas used for the estimates of SFR of HSB and LSB discs (central ellipse and a ring)

lower star formation rate than the HSB disc. The star forming ring (with the radius of approximately 50 arcsec) and bright centre have a SFR surface density comparable to the HSB disc: $(3.9 \pm 0.3) \times 10^{-3} M_{\odot} \text{ yr}^{-1} \text{ kpc}^{-2}$ and $(4.5 \pm 0.4) \times 10^{-3} M_{\odot} \text{ yr}^{-1} \text{ kpc}^{-2}$, respectively. We calculated the SFR density in the HSB disc: $(4 \pm 0.3) \times 10^{-3} M_{\odot} \text{ yr}^{-1} \text{ kpc}^{-2}$ and the elliptical ring encompassing the LSB part: $(1 \pm 0.1) \times 10^{-3} M_{\odot} \text{ yr}^{-1} \text{ kpc}^{-2}$ (the regions used for SFR estimates of HSB and LSB discs are shown in Fig. 5, right-hand column). The SFR surface density in the UGC 1378 LSB spiral arms is higher than for most LSB galaxies studied by (Wyder et al. 2009).

In Fig. 7 we compare UGC 1378’s SFR density vs gas surface density (the Schmidt–Kennicutt relation) to data in the literature. The gas surface density corresponds to H I calculated from the 0th moment map from Mishra et al. (2017) in the same areas as SFR density. Points for the HSB and LSB discs are plotted as black and gray circles, respectively. We plot the mean SFR and H I surface density for the entire galaxy with a large open circle. The black line corresponds to the relation with an exponent of 1.4 found by Kennicutt (1998). Triangles give results for LSB galaxies published by (Wyder et al. 2009), and bright and faint crosses show normal spiral galaxies from (Kennicutt 1998) – total and H I surface densities. A blue line shows the best-fitting relation for the H I surface density of Bluedisk galaxies from Roychowdhury et al. (2015). We also plot the SFR in the outer regions of spiral galaxies (Bigiel et al. 2010) (square symbols). In Fig. 7 the UGC 1378 measurements lie between normal spirals and LSB galaxies. The HSB disc data lie above the relation plotted for normal spirals, possibly indicating that the SFR is boosted by the bar driving gas to the star-forming rings. We cannot account for molecular gas since there are no available measurements for UGC 1378. The contribution of molecular gas

would likely move the HSB disc of UGC 1378 toward the locus of normal galaxies. Because the HSB SFR of UGC 1378 is close to the predicted SFR from the Kennicutt (1998) relation obtained from H I densities (faint crosses in Fig. 7). The LSB disc of UGC 1378 lies below the correlation and accounting for molecular gas would only increase the deviation from the normal Schmidt–Kennicutt relation. Similar deviations are observed in “classical” LSB galaxies, Bluedisk galaxies (Roychowdhury et al. 2015), outer parts of HSB spiral galaxies (Bigiel et al. 2010) and H I discs in early-type galaxies (Yildiz et al. 2017). These deviations for LSB galaxies are at least partially explained by their lower gas densities leading to lower SFRs (Abramova & Zasov 2011). A recent episode of gas accretion onto the disc of UGC 1378 may also contribute to a lower SFR if the gas is not yet fully participating in the star formation. Lutz et al. (2017) studied a sample of very H I rich galaxies and proposed that very high specific angular momentum in H I rich galaxies prevents the accreted gas from being transported to the mid-plane of the disc and being converted into stars. This mechanism may act to preserve giant gaseous discs.

4.2 On the formation scenario of UGC 1378

The radius of the HSB disc of UGC 1378, ~ 18 kpc, is comparable to the radius of the Milky Way’s disc. The normalized UGC 1378 SFR in this region is also comparable to the Milky Way SFR (for a Milky Way star formation radius of 13.5 kpc Chomiuk & Povich 2011). Hence, UGC 1378 resembles the Milky Way embedded in a gas-rich gLSB disc. Determining the formation scenario for this unusual system is an interesting challenge. The “Bluedisk” results

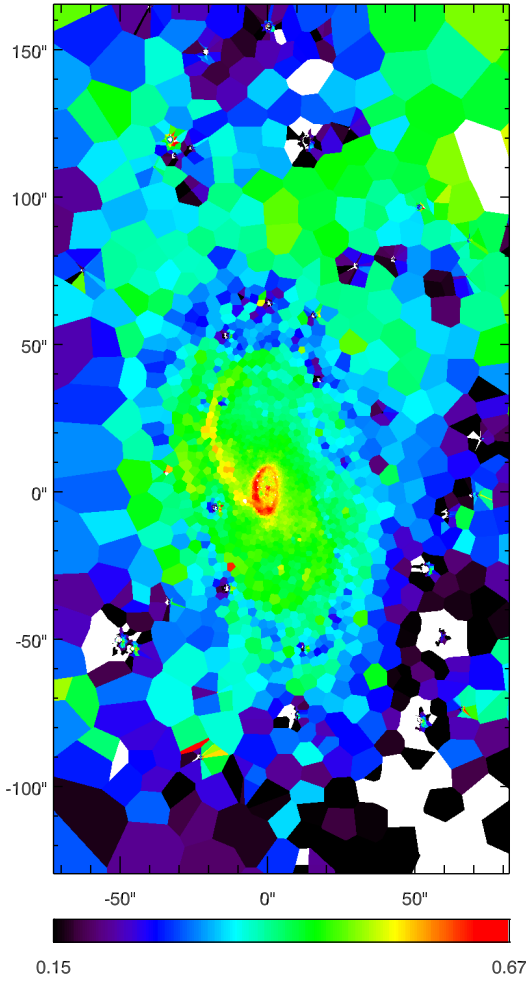


Figure 6. The $g-r$ colour map corrected for Galactic extinction. We masked a region affected by a Galactic cirrus in the bottom of the map. North is up, east is left.

indicate that H I-rich galaxies in some respects similar to UGC 1378 may accrete gas from an extended gas reservoir (Wang et al. 2015).

Saburova et al. (2018) suggested a three galaxy merger formation scenario for the giant LSB galaxy UGC 1922, which also have giant gaseous discs. The GALMER simulations (Chilingarian et al. 2010) of a major in-plane merger of two gas-rich bulgeless (e.g. Sd) galaxies also sometimes result in formation of a giant thin disc which might be classified as a gLSB. However, because the HSB disc of UGC 1378 is close to marginal gravitational stability, such a catastrophic formation scenario for UGC 1378 is unlikely, because otherwise the major merger would have heated the disc and increased stellar velocity dispersion. The unusually large radius of UGC 1378’s gaseous disc more likely results from two factors: a rich gas reservoir and an isolated environment that protects the disc from destruction by merger events. The fact that we observe UGC 1378 in isolation can indicate that it has been living in low density environment from the time of its formation and primary mass assembly because no mechanism can eject a large dark halo hosting a massive galaxy from a cluster or a rich group to a low density region of the Universe.

The blue colour and clumpy structure of the LSB spirals (see

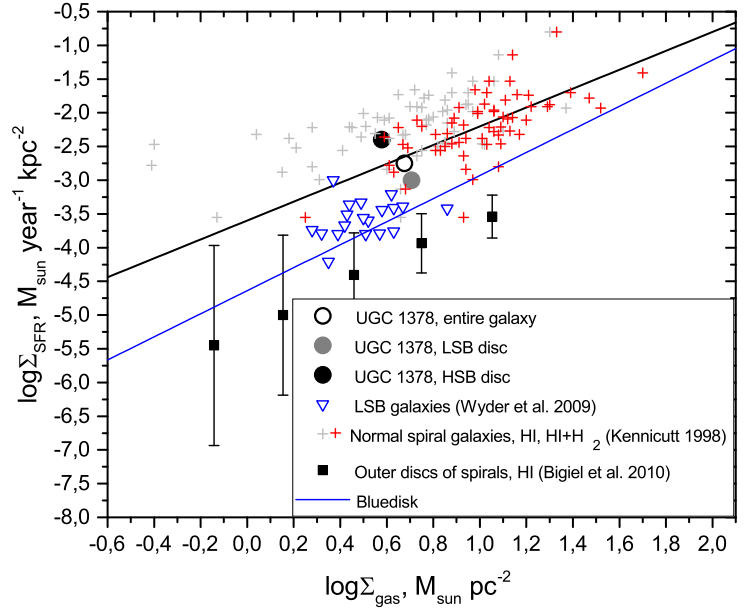


Figure 7. The SFR surface density vs gas surface density. The LSB and HSB discs of UGC 1378 are shown as gray and black circles, respectively, and the open circle denotes the mean value for the whole galaxy. The gas surface density for UGC 1378 is computed as the H I surface density from the 0th moment map from Mishra et al. (2017) corrected for the helium abundance. The sample of normal spirals from Kennicutt (1998) are plotted as bright and faint crosses correspond to total and H I gas densities, respectively. The black line corresponds to the fit by Kennicutt (1998). The blue line shows the fit for the Blue disk galaxies from Roychowdhury et al. (2015) for H I surface density. Triangles mark the position of LSB galaxies from the sample by Wyder et al. (2009). The estimates from Bigiel et al. (2010) for the outer parts of HSB spirals and H I surface density are shown as squares.

Fig. 6) suggest a recent burst of star formation in the LSB disc. The origins of a star burst in this low density region is puzzling, but may be the result of a recent minor merger. The variable obscuration in the foreground of UGC 1378 may hide traces of a putative merger event in our deep imaging data. Alternatively, the blue colour of the LSB disc may result from its low metallicity, consistent with slow accretion of gas from a cosmic filament.

The formation histories of well studied gLSB galaxies appear to be diverse if we include galaxies with properties intermediate between gLSB and HSB, particularly those with slightly smaller disc sizes like UGC 1378. While major mergers could be the likely origin of the most extended gLSBs like Malin 1 or UGC 1922 (Zhu et al. 2018; Saburova et al. 2018), this is not the case for UGC 1378.

5 CONCLUSIONS

We describe deep long-slit spectroscopy and imaging for UGC 1378, a galaxy with a giant H I and LSB disc. UGC 1378’s structure is complex, including a HSB pseudo-bulge and an HSB disc with a bar, rings and spiral arms, and a gas-rich gLSB disc with spiral arms and a radius of 50 kpc. We model UGC 1378’s stellar population and rotation curve and conclude that:

- (i) UGC 1378 resides between normal spirals and LSB galaxies in a SFR surface density vs gas surface density diagram. The LSB

disc has lower SFR surface density than expected from its gas density as for most gLSBs (Wyder et al. 2009) which may indicate recent gas accretion. The global SFR for UGC 1378 ($1.2 \dots 2.3 M_{\odot} \text{ yr}^{-1}$) is close to that of the Milky Way.

(ii) The stellar velocity dispersion of the HSB disc is close to that expected for its marginal gravitational stability, inconsistent with recent major merger events.

(iii) The dark matter halo dominates the mass inside the giant LSB disc radius. Within the HSB part of the galaxy the ratio of dark to luminous mass is close to 2 as expected for normal spirals.

(iv) We suggest that the formation of UGC 1378 occurred in two stages. The first stage, in common with MW-type galaxies, included several episodes of merging during which the HSB part formed and likely most satellites were accreted. In the second stage gLSB stellar and gaseous discs were formed by accretion of metal-poor gas from a cosmic filament. The unusually large radius of UGC 1378's gaseous disc could result from the presence of a gas reservoir (e.g. a cosmic filament). A low density environment likely helped to preserve the giant disc.

ACKNOWLEDGEMENTS

We are grateful to the anonymous referee for helpful comments. AS acknowledges The Russian Science Foundation (RSCF) grant 19-72-20089 that supported research on dynamical modelling of gLSBs and Russian Foundation for Basic Research grant 18-32-20120 that supported observational studies of star formation in disc galaxies. IC, AK and IK acknowledge the RScF grant 17-72-20119 for the reduction and analysis of spectral and photometric data. AS, IC, IK, and AK acknowledge the Leading Scientific School in astrophysics (direction: extragalactic astronomy) at Moscow State University. The authors are grateful to the staff of the MMT Observatory and of the Telescope Data Center at Smithsonian Astrophysical Observatory.

REFERENCES

Abramova O. V., Zasov A. V., 2011, *Astronomy Reports*, **55**, 202
 Afanasiev V. L., Moiseev A. V., 2005, *Astronomy Letters*, **31**, 194
 Bell E. F., McIntosh D. H., Katz N., Weinberg M. D., 2003, *ApJS*, **149**, 289
 Bertin E., Mellier Y., Radovich M., Missonnier G., Didelon P., Morin B., 2002, in Bohlender D. A., Durand D., Handley T. H., eds, *Astronomical Society of the Pacific Conference Series Vol. 281, Astronomical Data Analysis Software and Systems XI*. p. 228
 Bigiel F., Leroy A., Walter F., Blitz L., Brinks E., de Blok W. J. G., Madore B., 2010, *AJ*, **140**, 1194
 Boissier S., et al., 2008, *ApJ*, **681**, 244
 Boissier S., et al., 2016, *A&A*, **593**, A126
 Burkert A., 1995, *ApJ*, **447**, L25
 Cappellari M., Emsellem E., 2004, *PASP*, **116**, 138
 Chambers K. C., et al., 2016, preprint, p. [arXiv:1612.05560](https://arxiv.org/abs/1612.05560) ([arXiv:1612.05560](https://arxiv.org/abs/1612.05560))
 Chilingarian I., Prugniel P., Sil'Chenko O., Koleva M., 2007a, in Vazdekis A., Peletier R., eds, *IAU Symposium Vol. 241, IAU Symposium*. pp 175–176 ([arXiv:0709.3047](https://arxiv.org/abs/0709.3047)), [doi:10.1017/S1743921307007752](https://doi.org/10.1017/S1743921307007752)
 Chilingarian I. V., Prugniel P., Sil'Chenko O. K., Afanasiev V. L., 2007b, *MNRAS*, **376**, 1033
 Chilingarian I. V., Novikova A. P., Cayatte V., Combes F., Di Matteo P., Zasov A. V., 2009, *A&A*, **504**, 389
 Chilingarian I. V., Di Matteo P., Combes F., Melchior A.-L., Semelin B., 2010, *A&A*, **518**, A61
 Chomiuk L., Povich M. S., 2011, *AJ*, **142**, 197
 Chung A., Bureau M., 2004, *AJ*, **127**, 3192

Comerón S., Knapen J. H., Beckman J. E., Laurikainen E., Salo H., Martínez-Valpuesta I., Buta R. J., 2010, *MNRAS*, **402**, 2462
 Deeley S., et al., 2017, *MNRAS*, **467**, 3934
 Fabricant D., et al., 2019, arXiv e-prints,
 Fraternali F., Oosterloo T., Sancisi R., van Moorsel G., 2001, *ApJ*, **562**, L47
 Fraternali F., van Moorsel G., Sancisi R., Oosterloo T., 2002, *AJ*, **123**, 3124
 Freeman K. C., 1970, *ApJ*, **160**, 811
 Galaz G., Milovic C., Suc V., Busta L., Lizana G., Infante L., Royo S., 2015, *ApJ*, **815**, L29
 Geréb K., Janowiecki S., Catinella B., Cortese L., Kilborn V., 2018, *MNRAS*, **476**, 896
 Hagen L. M. Z., et al., 2016, *ApJ*, **826**, 210
 Huang S., et al., 2014, *ApJ*, **793**, 40
 Jarrett T. H., et al., 2013, *AJ*, **145**, 6
 Jedrzejewski R. I., 1987, *MNRAS*, **226**, 747
 Jester S., et al., 2005, *AJ*, **130**, 873
 Józsa G. I. G., 2007, *A&A*, **468**, 903
 Kansky J., et al., 2019, arXiv e-prints,
 Karachentsev I. D., Kaisin S. S., 2010, *AJ*, **140**, 1241
 Kasparova A. V., Saburova A. S., Katkov I. Y., Chilingarian I. V., Bizyaev D. V., 2014, *MNRAS*, **437**, 3072
 Katkov I. Y., Chilingarian I. V., 2011, in Evans I. N., Accomazzi A., Mink D. J., Rots A. H., eds, *Astronomical Society of the Pacific Conference Series Vol. 442, Astronomical Data Analysis Software and Systems XX*. p. 143 ([arXiv:1012.4125](https://arxiv.org/abs/1012.4125))
 Kennicutt Jr. R. C., 1998, *ApJ*, **498**, 541
 Khoperskov A. V., Zasov A. V., Tyurina N. V., 2003, *Astronomy Reports*, **47**, 357
 Kirby E. N., Rizzi L., Held E. V., Cohen J. G., Cole A. A., Manning E. M., Skillman E. D., Weisz D. R., 2016, preprint, ([arXiv:1610.08505](https://arxiv.org/abs/1610.08505))
 Kormendy J., Kennicutt Jr. R. C., 2004, *ARA&A*, **42**, 603
 Kregel M., van der Kruit P. C., 2004, *MNRAS*, **355**, 143
 Larson R. B., Tinsley B. M., Caldwell C. N., 1980, *ApJ*, **237**, 692
 Le Borgne D., Rocca-Volmerange B., Prugniel P., Lançon A., Fioc M., Soubiran C., 2004, *A&A*, **425**, 881
 Licquia T. C., Newman J. A., 2015, *ApJ*, **806**, 96
 Lutz K. A., et al., 2017, *MNRAS*, **467**, 1083
 Mishra A., Kantharia N. G., Das M., Omar A., Srivastava D. C., 2017, *MNRAS*, **464**, 2741
 Navarro J. F., Frenk C. S., White S. D. M., 1996, *ApJ*, **462**, 563
 O'Neil K., Bothun G. D., Cornell M. E., 1997, *AJ*, **113**, 1212
 Oosterloo T., Fraternali F., Sancisi R., 2007, *AJ*, **134**, 1019
 Peñarrubia J., McConnachie A., Babul A., 2006, *ApJ*, **650**, L33
 Peng C. Y., Ho L. C., Impey C. D., Rix H.-W., 2002, *AJ*, **124**, 266
 Rodriguez-Gomez V., et al., 2015, *MNRAS*, **449**, 49
 Roediger J. C., Courteau S., 2015, *MNRAS*, **452**, 3209
 Romeo A. B., Wiegert J., 2011, *MNRAS*, **416**, 1191
 Roychowdhury S., Huang M.-L., Kauffmann G., Wang J., Chengalur J. N., 2015, *MNRAS*, **449**, 3700
 Saburova A. S., 2011, *Astronomy Reports*, **55**, 409
 Saburova A. S., 2018, *MNRAS*, **473**, 3796
 Saburova A. S., Zasov A. V., 2013, *Astronomische Nachrichten*, **334**, 785
 Saburova A. S., Kasparova A. V., Katkov I. Y., 2016, *MNRAS*, **463**, 2523
 Saburova A. S., Katkov I. Y., Khoperskov S. A., Zasov A. V., Uklein R. I., 2017, *MNRAS*, **470**, 20
 Saburova A. S., Chilingarian I. V., Katkov I. Y., Egorov O. V., Kasparova A. V., Khoperskov S. A., Uklein R. I., Vozyakova O. V., 2018, *MNRAS*, **481**, 3534
 Salpeter E. E., 1955, *ApJ*, **121**, 161
 Saulder C., van Kampen E., Chilingarian I. V., Mieske S., Zeilinger W. W., 2016, *A&A*, **596**, A14
 Schlafly E. F., Finkbeiner D. P., 2011, *ApJ*, **737**, 103
 Schmidt P., Józsa G. I. G., Gentile G., Oh S.-H., Schubert Y., Ben Bekhti N., Winkel B., Klein U., 2014, *A&A*, **561**, A28
 Schombert J., 1998, *AJ*, **116**, 1650
 Seidel M. K., Falcón-Barroso J., Martínez-Valpuesta I., Díaz-García S., Laurikainen E., Salo H., Knapen J. H., 2015, *MNRAS*, **451**, 936
 Sersic J. L., 1968, *Atlas de galaxias australes*

- Shapiro K. L., Gerssen J., van der Marel R. P., 2003, *AJ*, **126**, 2707
- Stewart K. R., 2017, in Fox A., Davé R., eds, *Astrophysics and Space Science Library* Vol. 430, *Gas Accretion onto Galaxies*. p. 249 ([arXiv:1612.00513](https://arxiv.org/abs/1612.00513)), doi:10.1007/978-3-319-52512-9_11
- Tody D., 1986, in Crawford D. L., ed., *Society of Photo-Optical Instrumentation Engineers (SPIE) Conference Series* Vol. 627, *Instrumentation in astronomy VI*. p. 733
- Vollmer B., Nehlig F., Ibata R., 2016, *A&A*, **586**, A98
- Wang J., et al., 2013, *MNRAS*, **433**, 270
- Wang J., et al., 2015, *MNRAS*, **453**, 2399
- Wright E. L., et al., 2010, *AJ*, **140**, 1868
- Wyder T. K., et al., 2009, *ApJ*, **696**, 1834
- Yıldız M. K., Serra P., Peletier R. F., Oosterloo T. A., Duc P.-A., 2017, *MNRAS*, **464**, 329
- Zabl J., et al., 2019, *MNRAS*, **485**, 1961
- Zasov A. V., Khoperskov A. V., Tyurina N. V., 2004, *Astronomy Letters*, **30**, 593
- Zasov A. V., Khoperskov A. V., Saburova A. S., 2011, *Astronomy Letters*, **37**, 374
- Zasov A., Saburova A., Abramova O., 2015, *AJ*, **150**, 192
- Zhao D., Aragón-Salamanca A., Conselice C. J., 2015, *MNRAS*, **448**, 2530
- Zhu Q., et al., 2018, *MNRAS*, **480**, L18
- de Blok W. J. G., et al., 2014, *A&A*, **569**, A68
- den Heijer M., et al., 2015, *Astronomische Nachrichten*, **336**, 284
- van der Marel R. P., Franx M., 1993, *ApJ*, **407**, 525